

# DISTRIBUTION OF SHEAR STRAIN IN SQUARE CROSS-SECTION SHAFT MEASURED USING IMAGE ANALYSIS UNDER LARGE DEFORMATION

YASUYUKI KATO

*Dept of Mechanical Engineering, College of Science and Technology, Nihon University, Tokyo, Japan*

In the present study, the distribution of shear strain and warping in a square cross-section shaft generated under a large torsion is investigated using the image analysis based on the Natural Strain theory. The scribe lines are drawn in a grid on a surface of the test pieces made of natural rubber, and the image data of each element in the horizontal direction along the cross-section at the center and upper positions are taken by using a high-pixel camera equipped with macro lens. The distributions for shear strain and warping along the cross-section are obtained from that image data. These measured distributions under large deformation are compared with the distributions based on the conventional torsional theory of a square cross-section shaft, i.e., Saint Venant's theory for torsion. Moreover, taking the effect due to the elongation on the surface of specimens into consideration, the distributions modified elongation of gauge length are compared with experiments, and the validity of the present experimental results are confirmed in this paper.

*Keywords:* Finite deformation, Image data, Large torsion, Hyper-elastic body, Rubber, Warping, Rigid body rotation.

## 1 INTRODUCTION

The purpose of this research is to clarify the characteristics of finite strain, which is measured using image analysis as proposed in this paper. The Natural Strain theory used in this research has some merits that the associative law of strain can be satisfied, and the rigid body rotation can be clearly removed from shear strain component. Utilizing these merits to the method of image analysis, the measurements of the strain under a large deformation, which is generated on the surface of test pieces, are conducted in this research.

In the early stages of this research, in order to confirm the accuracy of the measurements based on the image analysis, the experiments for uniaxial tension, simple shear, and the combined load of them have been conducted by using the hollow cylindrical test pieces made of pure copper. Then, the adequacy of this image analysis was confirmed from the comparison with the results of conventional measurement using displacement mater (Kato and Futami 2013). However, these comparisons have been done only for uniform deformation fields where local deformation does not occur, and the experiments for larger deformation have not yet been examined in our early studies. Therefore, in our previous research, taking note of the larger deformation fields where local deformation occurs, the image analysis has been done, and the developing process of local deformation has been investigated under various loading histories (Kato 2015).

For the materials of the test pieces used in this study, a rubber is selected among hyper-elastic materials, and the distributions of shear strain and warping generated on the surface of a square cross-section shaft are examined under a large torsion. As for the torsion of shaft having a general cross-section other than a circular cross-section, the assumption that plane sections remain plane does not satisfy because the displacement in the axial direction arise with an increase of torsional deformation. Therefore, it is necessary to take into account warping in the torsional theory, and this is generally well known as Saint Venant's theory of torsion. However, since this theory applies only in the range of infinitesimal deformation, it is not always satisfied under a large deformation. On the other hand, as for the theory of the hyper-elastic materials for finite deformation, many analytical models are proposed (Rivlin 1948) and (Ogden 1972). However, much less work has been done on the researches for large torsion where the warping in a cross-section must be considered, and the details have not yet been clarified. Therefore, the distributions of shearing strains and longitudinal displacements in the cross-section are investigated based on the image analysis proposed in this research.

## 2 METHOD FOR DETERMINING DEFORMATION GRADIENT AND SHEAR STRAIN

This section explains the method for determining the principal strain, rigid body rotation, and shear strain based on the polar decomposition of deformation gradient. Figure 1 shows the relation between the current deformed state and initial undeformed state of three line elements which are located in the direction of  $\beta_{oa}$ ,  $\beta_{ob}$ ,  $\beta_{oc}$ , respectively. From the comparison between the initial undeformed and current deformed states of these line elements, components of deformation gradient, i.e., diagonal components ( $D_{11}$ ,  $D_{22}$ ) and off-diagonal components ( $D_{12}$ ,  $D_{21}$ ), can be derived. Moreover, the principal stretch  $\lambda_1$ , principal strain  $\varepsilon_1$ , current deformed direction  $\theta_m$ , undeformed direction  $\theta_o$ , and rigid body rotation  $\theta_R$  are represented in Eqs. (1) to (5) (Kato, 2015).

$$\lambda_1 = \frac{\sqrt{(D_{11} + D_{22})^2 + (D_{12} - D_{21})^2} + \sqrt{(D_{11} - D_{22})^2 + (D_{12} + D_{21})^2}}{2} \quad (1)$$

$$\varepsilon_1 = \ln \lambda_1 \quad (2)$$

$$\theta_m = \frac{\pi}{4} - \frac{1}{2} \tan^{-1} \left\{ \frac{D_{11}^2 + D_{12}^2 - D_{21}^2 - D_{22}^2}{2(D_{11}D_{21} + D_{12}D_{22})} \right\} \quad (3)$$

$$\theta_o = \frac{\pi}{4} - \frac{1}{2} \tan^{-1} \left\{ \frac{D_{11}^2 - D_{12}^2 + D_{21}^2 - D_{22}^2}{2(D_{11}D_{12} + D_{21}D_{22})} \right\} \quad (4)$$

$$\theta_R = \theta_o - \theta_m \quad (5)$$

Moreover, the shear strain on the vertical line element  $\ell_{oc}$  in the Natural Strain theory is defined by the pure angle, which is removed the rigid body rotation from the rotational angle of the vertical line element, and is represented in Eq. (6).

$$\gamma = \beta_{oc} - \beta_c - \theta_R \quad (6)$$

$$\text{where, } \beta_{oc} = \frac{\pi}{2} - \tan^{-1} \left\{ \frac{dX_c}{dY_c} \right\} \text{ and } \beta_c = \tan^{-1} \left\{ \frac{dy_c}{dx_c} \right\} = \tan^{-1} \left\{ \frac{D_{21} dX_c + D_{22} dY_c}{D_{11} dX_c + D_{12} dY_c} \right\}.$$

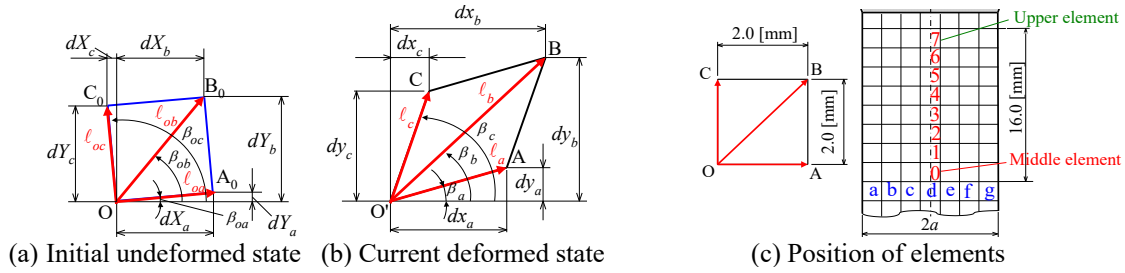


Figure 1. Three-line elements in a surface of test specimen.

### 3 EXACT SOLUTION BY SAINT VENANT'S THEORY

On the other hand, the exact solution of torsion based on the infinitesimal deformation theory is proposed by Saint Venant. The distributions of shear strain  $\gamma_{yz}$  and warping  $w$  for a square cross-section shaft are represented in Eq. (7) and Eq. (8) (Timoshenko and Goodier 1951).

$$\gamma_{yz} = \omega \left[ 2a - \frac{16}{\pi^2} \sum_{n=1,3,5}^{\infty} \frac{1}{n^2} (-1)^{(n-1/2)} \frac{\cosh(n\pi y/2a)}{\cosh(n\pi/2)} \sin(n\pi/2) \right] \quad (7)$$

$$w = \omega \left[ a y - \frac{32a^2}{\pi^3} \sum_{n=1,3,5}^{\infty} \frac{1}{n^3} (-1)^{(n-1/2)} \frac{\sinh(n\pi y/2a)}{\cosh(n\pi/2)} \sin(n\pi/2) \right] \quad (8)$$

Here,  $2a$  in Eq. (7) and Eq. (8) is a side length of the cross-section, and  $\omega$  is the angle of twist per unit length, and it is represented by using the values of twist angle  $\varphi_{deg}$  and initial gauge length  $L$  of test specimens in Eq. (9).

$$\omega = \frac{\pi \varphi_{deg}}{180 L} \quad (9)$$

### 4 EXPERIMENTAL CONDITIONS

The multi-axial loading test machine that can apply both axial displacement and torsional rotation at the same time is used to apply torsion with constraining axial displacement. Two high pixel cameras, with maximum effective pixels of 50.6 million, are used, and as shown in Figure 2(a), they are installed at the same distance. When taking the photographs of these elements, these cameras are rotating so that it is kept perpendicular to the surface of the specimen. Moreover, in order to measure each element in Figure 1(c), these cameras move from right to left or up and down. The test piece made of natural rubber (of hardness  $H_s = 65$ ) having a square cross-section, i.e.,  $14 \times 14$  [mm], and gauge length of 40 [mm] is used, as shown in Figure 2(b). And, this test piece is constrained by using an aluminum jig so that it would not be twisted at taper portions. As shown in Figure 1(c), the mark-off lines are drawn in advance with the same distance (2.0 [mm]) on the surface of the test piece. After attaching the test piece, the torsional moment is applied with constraining the axial displacement, with maximum torsional angles set to three stage, i.e.,  $\varphi_{deg} = 135, 225, 315$  [deg.]. The measurements of the image data have been carried out for eight elements from the middle to the upper position ( $N = 0 \sim 7$ ) and for seven elements in the horizontal direction at upper and middle positions (a~g).

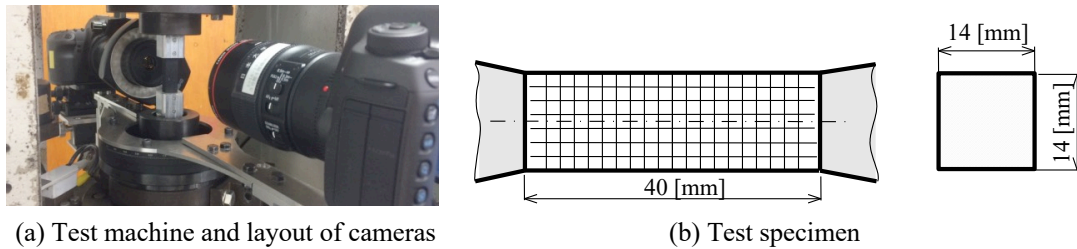


Figure 2. Experimental equipment and test specimen.

## 5 EXPERIMENTAL RESULTS AND DISCUSSION

### 5.1 Comparison of measurements at upper and middle position

Figure 3(a) shows the relation between the shear stress and the shear strain, which is measured at the upper position ( $N = 7$ ) and middle position ( $N = 0$ ) of element d in Figure 1(c) where the shear strain is maximum value. In this figure,  $A_0$  and  $A_7$  show the state at the twist angle  $\varphi_{deg} = 135$  [deg.],  $B_0$  and  $B_7$  show the state at  $\varphi_{deg} = 225$  [deg.], and  $C_0$  and  $C_7$  show the state at  $\varphi_{deg} = 315$  [deg.], respectively. Moreover, the green plots show the results measured at the upper position, and the red ones show the results measured at the middle. And, Figure 3(b) is a series of photographic images of their corresponding deformations. Since the red plots are larger than the green plots under the same stress condition, it is confirmed that the deformation at the middle position is more progress than the upper one. The black plots show the results of Saint Venant's theory obtained by the rotational angle of the test machine, and until state of A, it is almost the intermediate value between the red and green plots.

Figure 4 shows the distributions of shear strain along the cross-section at the upper and middle positions. In these figures, black solid lines represent the shear strain distribution derived by Saint Venant's theory (see Eq. (7)). The difference between the experimental results by the image analysis and the distribution by Saint Venant's theory is small in the state of A. However, the difference between them becomes larger in the state of C. Figure 5 shows the image photographs and the distributions of warping along the cross-section. Similarly, the difference between the results of the image analysis and distribution by Saint Venant's theory becomes larger in the state of C.

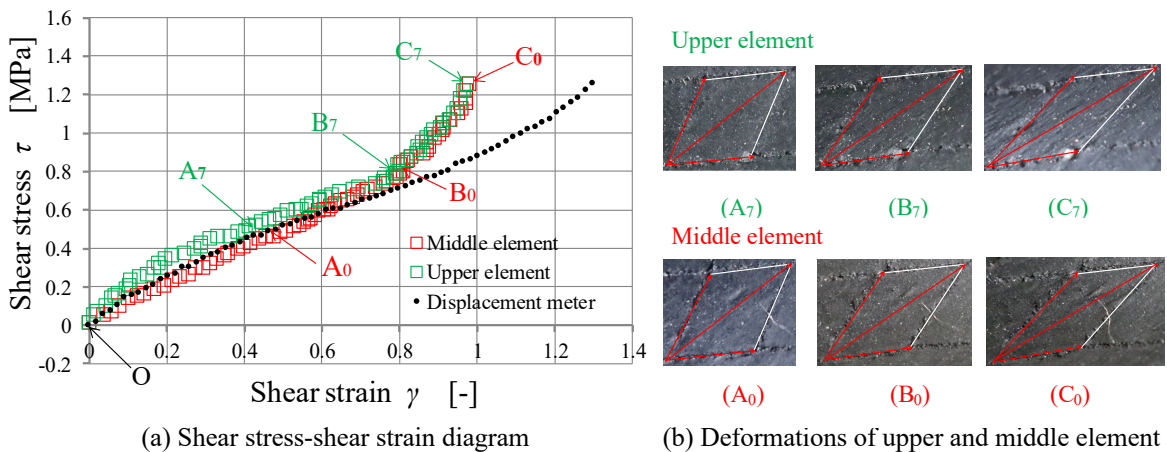


Figure 3. Relation between shear stress and shear strain.

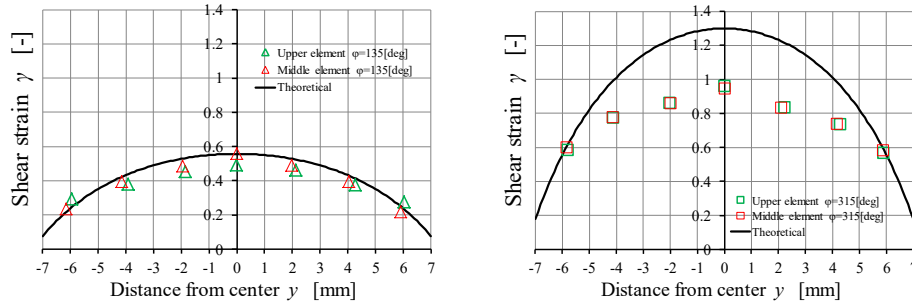


Figure 4. Distributions of shear strain in the state of A or C.

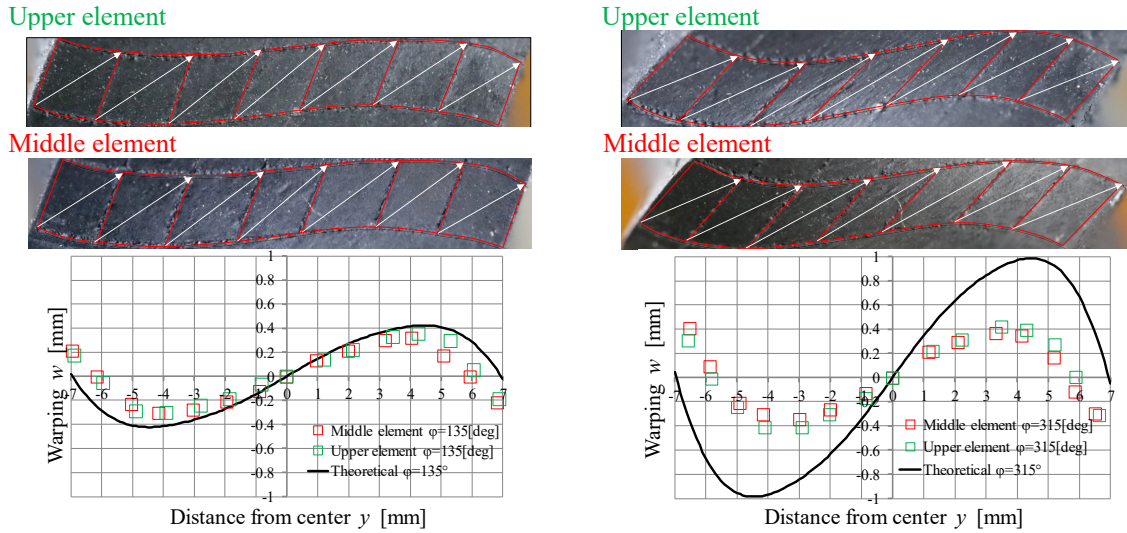
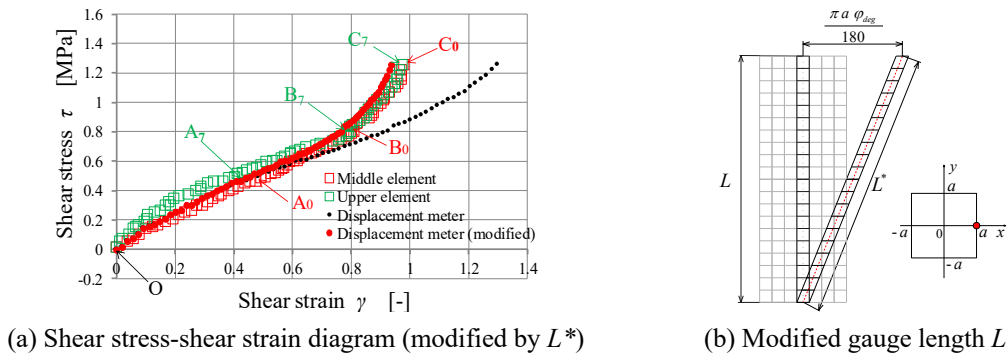


Figure 5. Distributions of warping in the state of A or C.

### 5.2 Modifications of elongation between gauge points and rigid body rotation

As shown in Figure 6(b), it is necessary to modify the gauge length in consideration of the current deformed configuration, and the modified gauge length  $L^*$  is represented in Eq. (10).

$$L^* = L \sqrt{1 + \left(\frac{\pi a \varphi_{deg}}{180L}\right)^2} \quad (10)$$



(a) Shear stress-shear strain diagram (modified by  $L^*$ )

(b) Modified gauge length  $L^*$

Figure 6. Comparison of modified theory with experimental results based on image analysis.

The red plots in Figure 6(a) show the modified results by  $L^*$ , and the modified results were found to agree well with the experiments of the image analysis. And, the red solid curves in Figure 7 show modified distributions for shear strain and warping, and these results were found to be closer to the experimental results. Moreover, the blue solid curve in Figure 7(b) represents the distribution that the effect of rigid rotation is considered further, and it becomes much closer to the experiments.

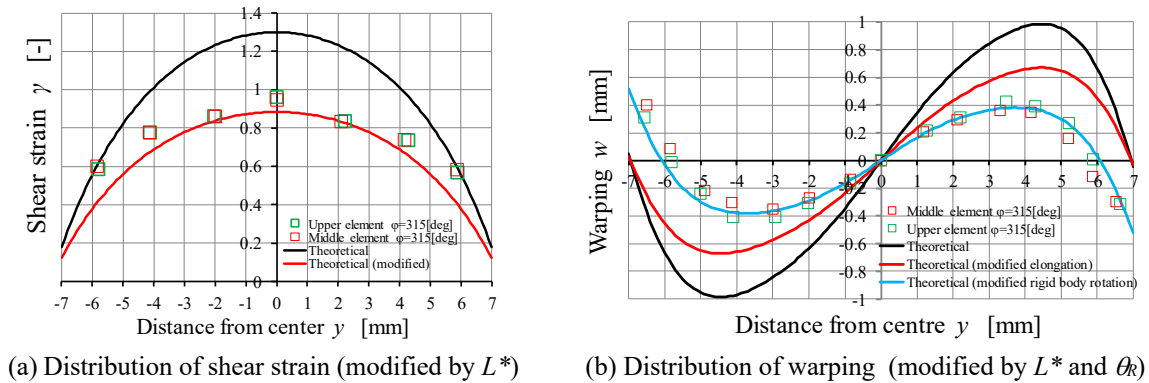


Figure 7. Modification of elongation and rigid body rotation in the state of C ( $\varphi_{deg} = 315$  [deg.]).

## 6 CONCLUDING REMARKS

The distributions of shear strain and warping generated in a square cross-section rubber shaft were investigated based on the image analysis in this study, and the following results were obtained.

- (1) In the relatively early stages of deformation, the increase in shear strain at the intermediate position progresses more compared to at the upper position.
- (2) From the comparison of the measurements by image analysis with the measurements based on the conventional Saint Venant's theory, it was revealed that the difference between them becomes larger as the torsional deformation increases.
- (3) Since the distributions of shear strain and warping, where the effects of elongation in gauge length and rigid body rotation are modified, become closer to those of this experiment, the validity and rationality of this image analysis were confirmed.

## References

- Kato, Y. and Futami, M., *Finite Strain Measurement Based on Image Analysis using Natural Strain (Measurement and Evaluation in Uniform Deformation Field)*, New Development in Structural Engineering and Construction, Yazdani, S. and Singh, A. (eds.), 1, 171-176, RPS Publishing, 2013.
- Kato, Y., *Image Analysis Based Finite Strain Measurement of Local Deformation under Uniaxial Loading Using Natural Strain*, Implementing Innovative Ideas in Structural Engineering and Project Management, N., Yazdani, S., and Singh, A (eds.), 1165-1170, ISEC Press, 2015.
- Ogden, R. W., *Large Deformation Isotropic Elasticity – On The Correlation of Theory and Experiment for Incompressible Rubberlike Solids*, Proceedings of the Royal Society of London. Series A: Mathematical and Physical Sciences, 326(1567), 565-584, 1972.
- Rivlin, R. S., *Large Elastic Deformations of Isotropic Materials. IV. Further Developments of the General Theory*, Philosophical Transactions of the Royal Society of London. Series A: Mathematical and Physical Sciences, 241(835), 379-397, 1948.
- Timoshenko, S. and Goodier, J. N., *Theory of Elasticity*, 2nd edition, McGraw-Hill, New York, 1951.